ACS APPLIED MATERIALS & INTERFACES

Research Article

www.acsami.org

Bifunctional Sensing Mechanism of SnO_2–ZnO Composite Nanofibers for Drastically Enhancing the Sensing Behavior in H_2 Gas

Akash Katoch,[†] Jae-Hun Kim,[†] Yong Jung Kwon,[‡] Hyoun Woo Kim,*[,‡] and Sang Sub Kim*[,†]

[†]Department of Materials Science and Engineering, Inha University, 100 Inha-ro, Incheon 402-751, Republic of Korea

[‡]Division of Materials Science and Engineering, Hanyang University, 17 Haengdamg Dong, 222 Wangsimni-ro, Seoul 133-791, Republic of Korea

Supporting Information

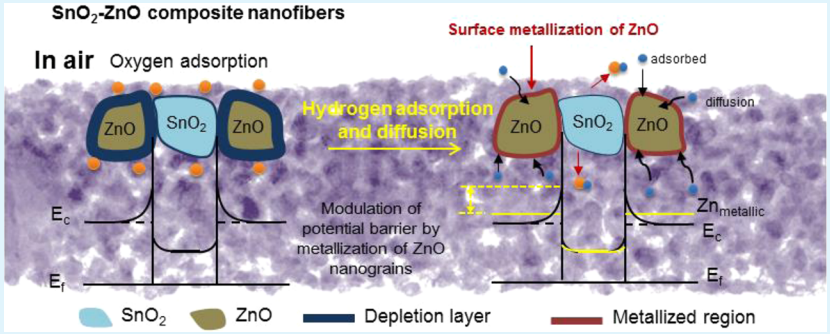

ABSTRACT: SnO_2–ZnO composite nanofibers fabricated using an electrospinning method exhibited exceptional hydrogen (H_2) sensing behavior. The existence of tetragonal SnO_2 and hexagonal ZnO nanograins was confirmed by an analysis of the crystalline phase of the composite nanofibers. A bifunctional sensing mechanism of the composite nanofibers was proposed in which the combined effects of SnO_2–SnO_2 homointerfaces and ZnO–SnO_2 heterointerfaces contributed to an improvement in the H_2 sensing characteristics. The sensing process with respect to SnO_2–ZnO heterojunctions is associated not only with the high barrier at the junctions, but also the semiconductor-to-metallic transition on the surface of the ZnO nanograins upon the introduction of H_2 gas.

KEYWORDS: *composite nanofibers, SnO_2, ZnO, sensors, hydrogen*

1. INTRODUCTION

In recent years, metal oxide nanofibers have attracted considerable interest for gas sensing applications because of their ease of fabrication, low processing cost, and, particularly, the presence of nanosized grains. The higher sensitivity with regard to the chemical sensors has been attributed to the behavior of grain boundaries formed at the interfaces of the nanograins, which exhibit a large change in resistance during adsorption and desorption of gas molecules.[1,2] Recent investigations have suggested that the microstructure of nanomaterials has a significant influence on gas sensing performance. Recently, the current authors reported that a ZnO fibrous structure was more favorable for detecting H_2 gas, in terms of employing the interesting hydrogen-induced metallization phenomenon in ZnO nanofibers, than were single crystalline nanowires.[3] The sensitivity to H_2 is enhanced by the formation of a large number of homojunctions among ZnO nanograins, exhibiting the semiconductor-to-metal conversion of their surfaces in the presence of H_2 molecules.[3,4]

This paper suggests that effective use of the above-mentioned metallization phenomenon toward the realization of high-performance H_2 sensors is reinforced by heterojunctions consisting of ZnO and another material. In particular, significant resistance modulation at the heterojunction provides a greater response during adsorption and desorption of H_2 gas molecules compared to that of their homojunction counterpart.[5] To date, several studies have observed enhanced sensor response from heterostructures, primarily due to the synergic effects of the two materials forming the heterojunctions.[6,7] After the selection of the most appropriate sensor material suitable for forming a heterojunction with ZnO, a sufficiently large difference in resistance is observed in the absence of H_2 gas in conjunction with an extremely low resistance upon exposure to H_2 gas.

Several metal oxide semiconductors, such as SnO_2, TiO_2, In_2O_3, and WO_3, have potential as H_2 sensors. Among them, SnO_2 was chosen in this study for the following reasons. SnO_2 has a large bandgap of 3.56 eV at 300 K and a high carrier concentration of up to 5.70×10^{20} cm^{-3},[8] making it an excellent candidate for gas sensors. Furthermore, SnO_2 has been the dominant choice for domestic, commercial, and industrial settings due to the low operating temperatures.[9]

Received: February 27, 2015
Accepted: May 7, 2015
Published: May 7, 2015

DOI: 10.1021/acsami.5b01817
ACS Appl. Mater. Interfaces 2015, 7, 11351–11358

Despite its excellent sensor response, the most serious disadvantage of the SnO_2 sensor is its poor selectivity.[10] Accordingly, the present study attempted to circumvent this limitation by providing many ZnO-based heterostructures.

In this study, H_2 sensing behavior was significantly enhanced through the use of SnO_2–ZnO heterostructures. Thus far, SnO_2–ZnO heterostructures have been used widely to detect various types of reducing and oxidizing gases.[7,11] The heterostructure was fabricated as one-dimensional nanofibers composed of nanosized ZnO and SnO_2 grains. First, the adsorbed hydrogen generates a metallic thin layer on the boundaries of the ZnO nanograins, drastically enhancing the sensitivity and selectivity to H_2 gas due to the SnO_2–ZnO heterointerfaces. Second, the SnO_2 nanograins contribute to the sensing behavior through the formation of SnO_2–SnO_2 homointerfaces and SnO_2–ZnO heterointerfaces. Overall, this paper reports a bifunctional mechanism of H_2 sensing in regard to SnO_2–ZnO composite nanofibers.

2. EXPERIMENTAL DETAILS

2.1. Materials. Tin(II) chloride dihydrate ($SnCl_2{\cdot}2H_2O$, Sigma-Aldrich Corp.), zinc acetate ($Zn(OAc)_2$, Sigma-Aldrich Corp.), polyvinylpyrrolidone (PVP, M_w = 1 300 000, Sigma-Aldrich Corp.), poly(vinyl alcohol) (PVA, M_w = 80 000, Sigma-Aldrich Corp.), ethanol (anhydrous, 99.5%, Sigma-Aldrich Corp.), dimethylformamide (DMF, anhydrous, 99.8%, Sigma-Aldrich Corp.), and deionized water were used as the precursor materials.

2.2. Synthesis of SnO_2–ZnO Composite Nanofibers. The composition of the prepared electrospinning solution was xZnO–$(1-x)SnO_2$ (x = 0.01–0.50). In a typical process, 1.4 g of $SnCl_2{\cdot}2H_2O$ and 0.35 g of $Zn(OAc)_2$ were dissolved in a mixed solvent consisting of DMF and ethanol at a 1:1 ratio with constant stirring for 1 h. Subsequently, 8 wt % of PVP was added to the Sn–Zn precursor solution and was stirred for 10 h. The prepared viscous solution was loaded into a syringe equipped with a 21-gauge stainless steel needle (inner diameter = 0.51 mm). The distance between the tip of the needle (15 kV) and the grounded collector was set to 20 cm. The solution was fed at 0.05 mL/h using an accurate syringe pump at room temperature in air. The as-spun nanofibers were produced on a SiO_2 layer-coated Si wafer placed on the collector region. The as-spun nanofibers were then calcined at 700 °C in air for 0.5 h at a heating rate of 0.5 °C/min. We obtained highly crystalline SnO_2 and ZnO phases in composite nanofibers through calcination at 700 °C. Further, at this same temperature, complete removal of PVP and PVA polymer was observed. In addition, SnO_2 and ZnO nanofibers were also synthesized individually via the same electrospinning process using PVP and PVA polymers. The detailed procedure for the synthesis of SnO_2 and ZnO nanofibers is reported elsewhere.[12,13] Both the SnO_2 and ZnO nanofibers were calcined under the same conditions used for the SnO_2–ZnO composite nanofibers.

2.3. Microstructural Analysis and Sensing Measurements. The samples were analyzed by field-emission scanning electron microscopy (FE-SEM, Hitachi S-4200), transmission electron microscopy (TEM, Philips CM-200) equipped with an energy-dispersive X-ray spectrometer (EDX), and X-ray diffraction (XRD, Philips X'pert MRD diffractometer). Furthermore, as electrodes for the sensing measurements, Au (thickness ~200 nm) and Ti (thickness ~50 nm) layers were sequentially sputter-deposited on the specimens using an interdigitated electrode mask similar to those reported previously.[14−16] The fabrication of sensor device is illustrated in Figure S1, Supporting Information. The response of the composite nanofiber sensors to H_2 was measured using a custom-made gas dilution and sensing system. In a typical experiment, a known amount of highly purified H_2 (>99.999%) was introduced into the sensing chamber. The H_2 concentrations, which were obtained using N_2 gas as a diluting agent, were in the range 0.1–10 ppm. Dynamic resistance curves and corresponding sensor responses of the $0.90SnO_2$–0.10ZnO nanofiber sensor were measured at different temperatures, as shown in Figure S2, Supporting Information. The sensor was most sensitive at 300 °C; accordingly, the operating temperature was optimized to 300 °C. The total gas flow rate was set to 500 sccm. Sensor response was used to evaluate the sensing capability, which is defined as R_a/R_g, where R_a is the initial resistance of the sensor (absence of H_2 gas), and R_g is the resistance of the sensor in the presence of H_2 gas. The response and recovery times were defined as the time taken for the resistance to change by 90% upon the introduction and removal of H_2 gas, respectively.[17]

3. RESULTS AND DISCUSSION

The microstructures of the SnO_2–ZnO composite nanofibers were observed using FE-SEM (Figure 1a–h). The insets show

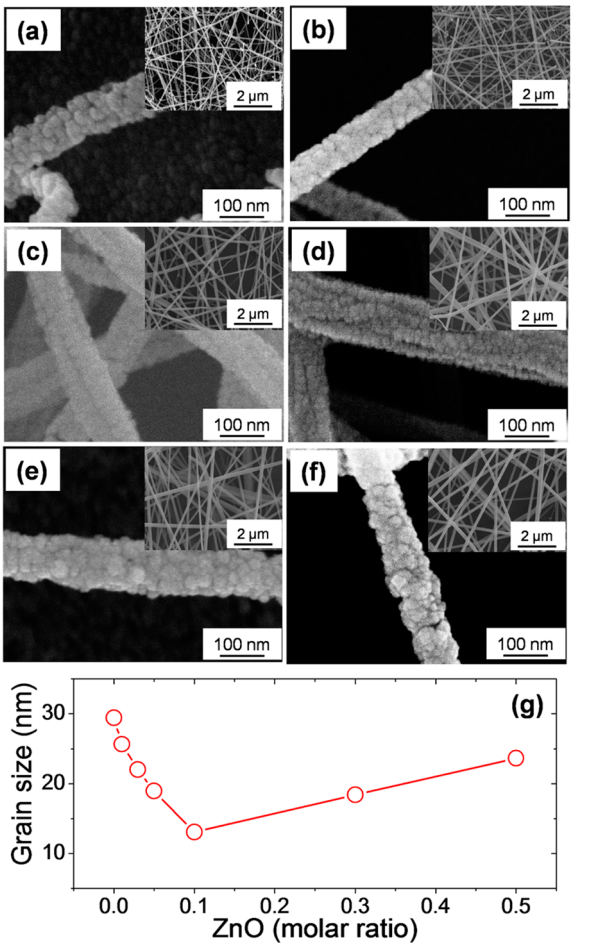

Figure 1. FE-SEM images of the $(1-x)SnO_2$–xZnO composite nanofibers with different ZnO contents: x = (a) 0.01, (b) 0.03, (c) 0.05, (d) 0.10, (e) 0.30, and (f) 0.50. (g) Grain size of the different nanofibers analyzed in this study.

the low-magnification images, illustrating that the nanofibers were distributed randomly and uniformly over the substrate. Figure 1g summarizes the mean grain sizes of the SnO_2–ZnO composite nanofibers compared to those of the SnO_2 nanofibers. Here, the mean grain size refers to the average of the composite nanofibers measured by SEM; thus, it is the average size of all grains in the nanofibers, in which SnO_2 and ZnO grains cannot be distinguished from each other. The mean size of the nanograins in the SnO_2–ZnO composite nanofibers was significantly reduced by increasing the ZnO molar ratio from 0.01 to 0.1; however, further increases in the molar ratio

DOI: 10.1021/acsami.5b01817
ACS Appl. Mater. Interfaces 2015, 7, 11351–11358

from 0.30 to 0.50 increased the grain size. This suggests that the addition of ZnO affects the growth of the nanograins, leading to the observed decrease in grain size compared to the pure SnO_2 nanofibers. On the other hand, the diameter of the composite nanofiber was not significantly affected by the addition of ZnO to SnO_2. The mean diameter of electrospun-synthesized nanofibers was estimated to be approximately 90 nm, irrespective of the ZnO content.

The microstructure of SnO_2–ZnO composite nanofibers was investigated further using TEM (Figure 2). The low-

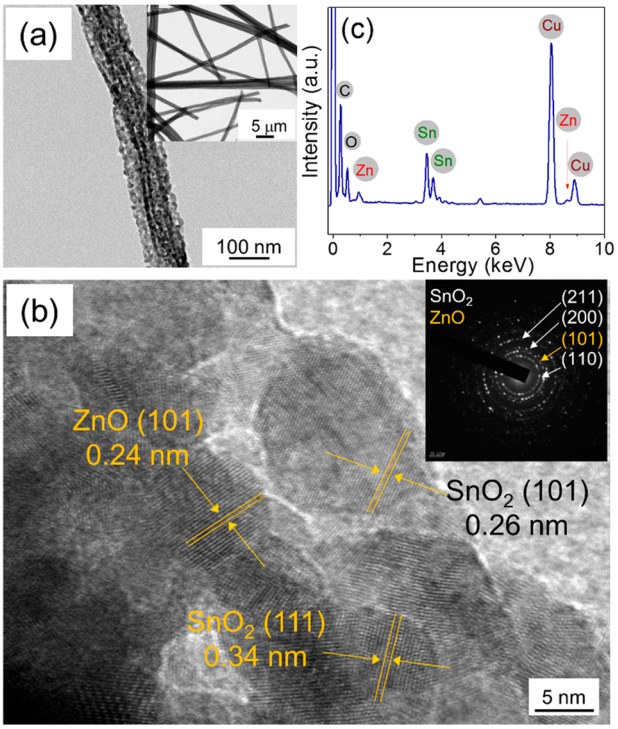

Figure 2. (a) TEM image of a single $0.9SnO_2$–$0.1ZnO$ nanofiber (inset: low-magnification TEM image). (b) Corresponding high-resolution TEM image. The inset shows a representative SAED pattern. (c) EDS spectrum of the $0.9SnO_2$–$0.1ZnO$ nanofiber.

magnification TEM image in Figure 2a clearly shows the presence of smaller-sized nanograins in a single nanofiber; a typical nanofiber was selected from the sample shown in the upper-right inset of Figure 2a. This is in good agreement with the FE-SEM image shown in Figure 1d. The high-magnification TEM image of the composite nanofiber shown in Figure 2b reveals the coexistence of ZnO and SnO_2 nanocrystals. The interplanar distance of 0.24 nm, as determined from the high-magnification TEM image, corresponds to the (101) plane of hexagonal ZnO. In addition, the lattice spacings of 0.26 and 0.34 nm correspond to the (101) and (110) planes of tetragonal SnO_2, respectively. The selected area diffraction pattern of the composite nanofibers, shown as an inset in the figure, clearly reveals the polycrystalline nature of the nanograins. The heterojunctions are formed at the interface between the SnO_2 and ZnO nanograins in the composite nanofibers. EDX element mapping (Figure 2c) confirmed the presence of Zn, Sn, and O in the composite nanofibers.

Furthermore, the crystalline phase of the SnO_2–ZnO composite nanofibers was examined using XRD (Figure 3). A set of peaks matching the tetragonal rutile structure of SnO_2 were observed (JCPDS Card No. 88-0287). The XRD pattern

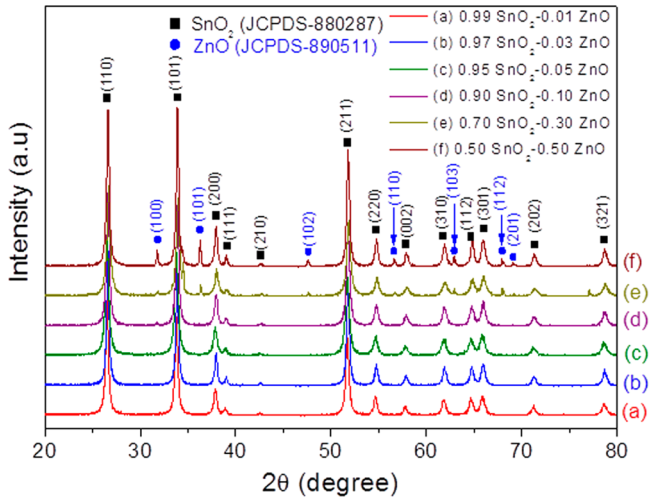

Figure 3. XRD patterns of SnO_2–ZnO composite nanofibers with different ZnO molar ratios.

of the SnO_2–ZnO composite nanofibers exhibited additional peaks related to the hexagonal structure of ZnO (JCPDS Card No. 88-0511). The existence of a ZnO phase confirms the presence of ZnO nanograins in the composite nanofibers. On the other hand, the intensity of the ZnO peaks was relatively low, indicating a relatively small amount of ZnO structure in the composite nanofibers. Further detailed analysis is shown in Figure S3 and Text S1, Supporting Information.

The sensing capabilities of the composite nanofibers were tested. Figure S4, Supporting Information, presents the dynamic resistance curves of the sensors at 300 °C. The H_2 gas concentrations were set to 0.1, 1, 5, and 10 ppm. The ZnO molar ratios were set to 0.01, 0.03, 0.05, 0.10, 0.30, and 0.50. The resistance decreased or increased with the introduction or removal of H_2, respectively. The SnO_2–ZnO composite nanofiber sensor showed significantly better H_2-sensing behavior than that of the pure SnO_2 nanofibers, which could be attributed to the special interplay between ZnO and SnO_2. Figure 4a,b presents the responses of all SnO_2–ZnO composite nanofiber sensors. The corresponding response and recovery times are summarized in Table S1, Supporting Information, revealing no significant changes in these times with varying gas concentrations.

According to a previous study,[3] ZnO nanofibers are more sensitive to H_2 than are SnO_2 nanofibers. The dynamic resistance curves and sensor responses of the composite nanofibers were compared of those of pure SnO_2 and ZnO nanofibers (Figure 4c,d). For example, at 10 ppm, the sensor responses of pure ZnO nanofibers, pure SnO_2 nanofibers, and $0.90SnO_2$–$0.10ZnO$ composite nanofibers were 63.8, 4.2, and 168.6, respectively. At H_2 concentrations in the range 0.1–10 ppm, the pure SnO_2 nanofibers exhibited the lowest sensitivity, whereas the $0.90SnO_2$–$0.10ZnO$ composite nanofiber sensor exhibited the highest response among all the sensors; however, a further increase in the ZnO molar ratio to 0.30 and 0.50 gradually decreased the response. Figure 4e shows the responses of the SnO_2–ZnO composite nanofiber sensors to 0.1 ppm of H_2 according to the ZnO molar ratio.

The sensing response was significantly improved by the addition of ZnO nanograins to the SnO_2 nanofibers. The composite nanofiber sensors with a ZnO molar ratio of 0.10 showed the highest response, indicating that the ZnO content

DOI: 10.1021/acsami.5b01817
ACS Appl. Mater. Interfaces 2015, 7, 11351–11358

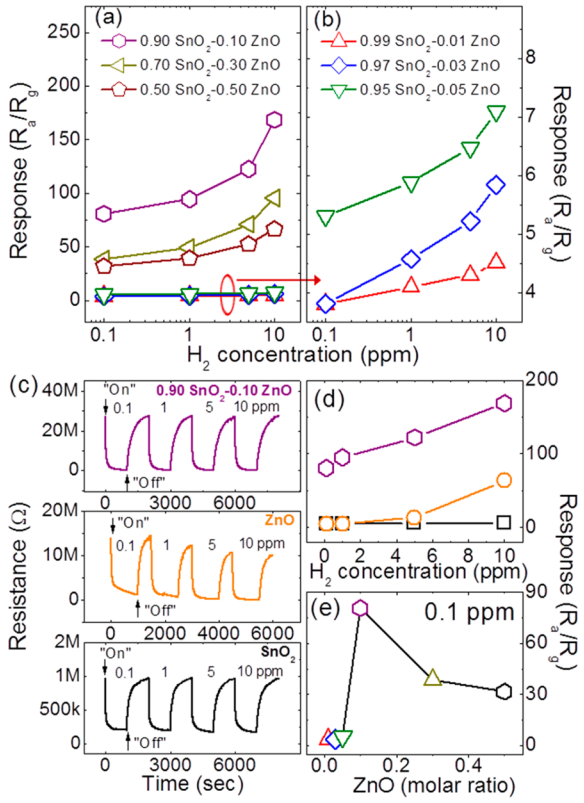

Figure 4. (a, b) Summary of the sensor responses of SnO_2–ZnO composite nanofibers. (c) Dynamic resistance curves of pure ZnO, pure SnO_2, and SnO_2–ZnO composite nanofibers for 0.1–10 ppm of H_2. (d) Variations of the sensor responses of the pure ZnO, pure SnO_2, and SnO_2–ZnO composite nanofibers with varying H_2 concentrations. (e) Sensor responses of the SnO_2–ZnO composite nanofibers to 0.1 ppm of H_2 according to the ZnO content.

should be optimized to obtain the best H_2-sensing properties in SnO_2–ZnO composite nanofiber sensors. Furthermore, the sensitivity of the composite sensor to H_2 was compared with those of the other gases, including CO, benzene, and toluene, all at concentrations of 10 ppm. Figure 5a shows the corresponding normalized resistance curves. As is evident, the SnO_2–ZnO composite nanofibers showed the strongest response to H_2 compared to its response to other gases. Figure 5b shows the corresponding bar graph comparing the sensor responses of the composite nanofibers to the four gases.

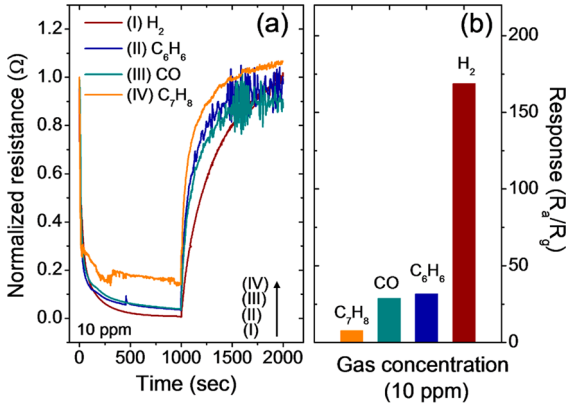

Figure 5. (a) Normalized dynamic resistance curves and (b) responses of the $0.9SnO_2$–0.1ZnO nanofibers to 10 ppm of various reducing gases at 300 °C.

A bifunctional sensing mechanism is proposed to explain the improved sensing behavior of SnO_2–ZnO composite nanofibers to H_2 gas. The bifunctional sensing mechanism included the following: (1) reducing the gas effect between the neighboring SnO_2 nanograins and (2) a metallization effect between the ZnO and SnO_2 nanograins. The first mechanism (m_1) corresponds to a grain-boundary-dependent phenomenon exhibited by SnO_2 homojunctions, as shown in Figure 6a. Being similar to the pure SnO_2 nanofibers, many SnO_2 homojunctions exist between two adjacent nanograins in the composite nanofibers. In air, oxygen molecules diffuse through the nanograins and completely cover the grain boundaries. The oxygen molecules adsorbed on the surfaces of the SnO_2 nanograins extract electrons from the nanograins and form potential barriers between the adjacent nanograins, which restrict the flow of electrons through the nanograins. During H_2 exposure, the H_2 molecules interact with chemisorbed oxygen species and release electrons with the concomitant generation of H_2O. The electrons released back to the SnO_2 nanograins reduce the height of the potential barrier established at the grain boundary, resulting in resistance modulation at the SnO_2–SnO_2 homojunctions.

On the other hand, in the case of SnO_2–ZnO composite nanofibers, some potential barriers are generated between the neighboring SnO_2 and ZnO nanograins. Note that the addition of ZnO to SnO_2 nanofibers reduced the grain size (Figure 1). These smaller nanograins also contribute to sensor enhancement because the area of the grain boundaries is increased. The grain size of the pure nanofibers is decreased by approximately 55% upon the addition of ZnO in order to prepare the $0.90SnO_2$–0.10ZnO composite nanofiber. On the other hand, at 10 ppm, the corresponding sensor response was increased from 4.2 to 168. Accordingly, the decrease in grain size cannot account for the drastic sensor enhancement observed in the present work. The second mechanism (m_2) of the ZnO–SnO_2 heterojunctions contributes to the enhanced sensor response (Figure 6b). Figure S5, Supporting Information, shows the energy band diagram of the heterojunction formed at the boundaries between the SnO_2 and ZnO nanograins.[18] When an n-SnO_2 nanograin comes into contact with an n-ZnO nanograin, the difference in electron workfunction results in the unidirectional flow of electrons, ultimately equating the Fermi levels of the two materials. This results in bending of the energy band and vacuum energy level at the ZnO/SnO_2 interfaces. The heterojunction enhances the sensing abilities by promoting the modulation of resistance (or electron concentration).[7,12,15,16,19] Several researchers have fabricated a range of sensors based on ZnO–SnO_2 composites. For example, sensors composed of ZnO nanorods modified with SnO_2 nanoparticles[20] and SnO_2–ZnO hybrid nanofibers[11] were shown to exhibit a strong response to NO_2 gas. This was explained on the basis of charge transfer at the ZnO/SnO_2 interfaces.[11,20] Similarly, the sensors fabricated with mesoporous ZnO–SnO_2 nanofibers were found to be sensitive to ethanol gas.[7] This was explained by considering the surface depletion effect at the heterointerface.[7] Moreover, the sensing characteristics also depend on the nature of the chemical species and their interactions with oxide materials. For example, it was reported that the mechanism underlying the sensing characteristics of SnO_2–ZnO composites to ethanol gas is closely related to the decomposition and oxidation of ethanol

DOI: 10.1021/acsami.5b01817
ACS Appl. Mater. Interfaces 2015, 7, 11351–11358

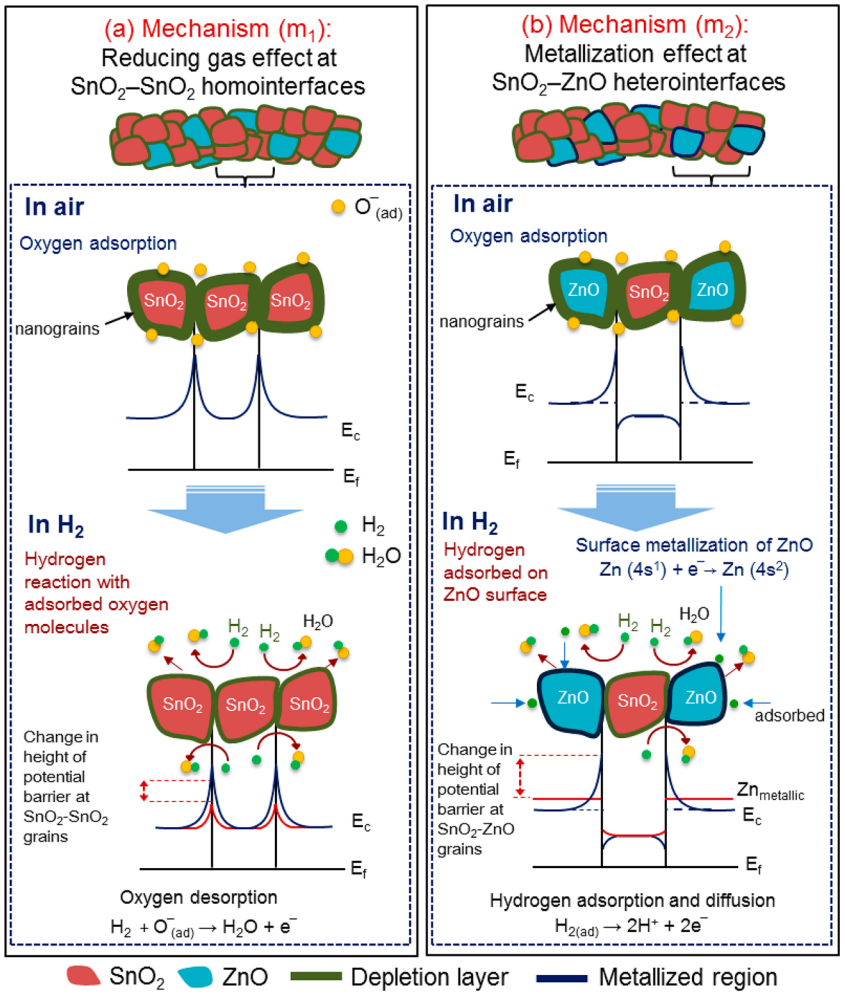

Figure 6. Schematic diagram of the proposed bifunctional sensing mechanism, explaining the enhanced sensitivity of the SnO_2–ZnO composite nanofibers to H_2. (a) Mechanism (m_1): reducing gas effect at SnO_2–SnO_2 homointerfaces. (b) Mechanism (m_2): metallization effect at SnO_2–ZnO heterointerfaces.

with the acid–base catalytic properties of SnO_2 and ZnO.[21,22] Ethanol undergoes different reactions depending on the material properties of the surface (i.e., ZnO or SnO_2).

The second mechanism (m_2) proposed in this study mainly involves the additional modulation of resistance between the neighboring ZnO and SnO_2 nanograins, resulting from the surface metallization of ZnO grains in the presence of H_2 (Figure 6b). According to previous experimental and theoretical studies, metallization of the ZnO surface occurs by the adsorption of hydrogen atoms on the O sites of the nonpolar surfaces of ZnO.[23,24] Recently, the surface metallization of ZnO nanofibers in the presence of H_2 molecules was examined using XPS,[3] which can be applied to the present case of composite nanofibers. According to XPS, the inferred spin–orbit splitting for Zn^{2+} = 23.0 eV changed to Zn^0 = 23.1 eV. In addition, the Zn 2p features shifted to a lower binding energy upon exposure to H_2, confirming the metallization of the ZnO surface.[25−30] The reason for the metallization of the ZnO surface can be understood in terms of the interaction of H_2 with the lattice oxygen of ZnO. Strong hybridization occurs between the s-orbitals of H and the p-orbitals of O, where the O-p energy states located at the Fermi level shifted to a lower energy. Because of the strong hybridization between the H-s and O-p orbitals, charge delocalization occurs between Zn and the O–H bond and partially occupies the 4s and 3d states of the surface Zn atoms.[25] This charge delocalization metallizes the surface Zn atoms, where the 4s and 3d states of Zn contribute to the electrical conduction.

Accordingly, upon exposure to H_2 gas, a semiconductor-to-metallic transformation of the ZnO surface occurs. The heterojunction between ZnO and SnO_2 is destroyed because of the semiconductor (ZnO)-to-metallic (Zn) transition of the ZnO surface and the accelerated electron transport from the metallic Zn ($\varphi_{(Zn)}$ = 4.3 eV) surface to SnO_2. This reduces the overall resistance of the sensor. When H_2 gas is removed and air is supplied, the metal Zn recovers to ZnO, thereby re-establishing the original band configuration. This semiconductor-to-metallic surface transition in ZnO significantly increases the modulation of resistance.

The highest response was obtained from composite nanofibers with the molar ratio of Sn to Zn at 9:1. The additional modulation of resistance in composite nanofibers results from the transition of semiconductor (SnO_2)–semiconductor (ZnO) heterojunction to semiconductor (SnO_2)–metal (Zn) in the presence of H_2. When the content of ZnO exceeds the critical amount, some ZnO nanograins will be in contact, in which electrons will pass through metallic–metallic (Zn) contact formed between boundaries of two adjacent ZnO grains, lowering the modulation of resistance. On the other hand, when the ZnO content is lower than its critical amount,

DOI: 10.1021/acsami.5b01817
ACS Appl. Mater. Interfaces 2015, 7, 11351−11358

Table 1. Gas Sensing Abilities of SnO_2–ZnO Composite Materials

nanostructure type	gas	gas conc (ppm)	T (°C)	response (R_a/R_g or R_g/R_a)	ref
ZnO–SnO_2 nanocomposites	NO_2	500	250	34.5	31
SnO_2–ZnO core–shell nanofibers	O_2	70	300	1.2	32
	NO_2	5	300	1.4	32
SnO_2–ZnO composite nanofibers	NO_2	4	200	105	33
ZnO–SnO_2 core–shell nanowires	NO_2	10	200	66.3	34
	ethanol	200	400	280	34
SnO_2–ZnO composite thin films	ethanol	200	300	4.69	35
mesoporous SnO_2–ZnO composite nanofibers	ethanol	50	300	12.8	36
ZnO-branched SnO_2 nanowires	ethanol	100	400	6.2	37
ZnO-doped SnO_2 nanoparticles	ethanol	300	250	3900	38
	CO	500	200	1020	38
ZnO–SnO_2 composites	CO	200	350	12	39
hollow hierarchical SnO_2–ZnO composite nanofibers	methanol	10	350	8.7	40
SnO_2 nanoparticles doped with ZnO microrods	trimethylamine	50	330	125	41
SnO_2-coated ZnO nanorods	H_2	500	400	1.7	42
ZnO-coated SnO_2 nanorods	H_2	100	350	18.4	43
ZnO-SnO_2 composite films	H_2	10 000	150	1.9	44
SnO_2–ZnO composite nanofibers	H_2	10	300	168.6	present work

the number of SnO_2–ZnO heterojunction will be insufficient. Subsequently, the metallization effect will be decreased.

To date, a variety of SnO_2–ZnO composite materials have been developed to detect various gases (Table 1[31−44]). Although several researchers have reported a very high response at a gas concentration higher than 100 ppm, it is not common to fabricate sensors operating at a low concentration of 10 ppm or below. For NO_2 gas, the sensors fabricated from SnO_2–ZnO composite nanofibers,[33] SnO_2–ZnO core–shell nanofibers,[32] and ZnO-SnO_2 core–shell nanowires[34] exhibited sensor responses of 105 (4 ppm), 1.4 (5 ppm), and 66.3 (10 ppm), respectively. Recently, Tang et al. obtained a methanol gas sensor response of 8.7 at 10 ppm using the hollow hierarchical SnO_2–ZnO composite nanofibers.[40] Furthermore, a few studies have reported H_2 sensor behavior of SnO_2–ZnO composite materials. The SnO_2-coated ZnO nanorods exhibited a sensor response of 1.7 at 500 ppm,[42] whereas the ZnO-coated SnO_2 nanorods exhibited a sensor response of 18.4 at 100 ppm.[43] Mondal et al. obtained a H_2 gas sensor response of 1.9 at 10 000 ppm using ZnO–SnO_2 composite films.[44] Although Zn nanopillars exhibited a high sensor response of 70 at a H_2 concentration of 2500 ppm,[45] most ZnO nanostructures showed sensor responses lower than 10 (Table 1 in ref 3). In comparison, ZnO nanofibers exhibited a much larger response of 109.1 at a low concentration of 10 ppm.[3] Thus, the large number of homojunctions between nanograins in the nanofiber structure will contribute to the significant enhancement in sensor behavior. On the other hand, pure SnO_2 nanofibers showed no noticeable H_2 sensitivity at 10 ppm.[3] The SnO_2 nanoparticle-based thin films exhibited a very high sensor response (~660) at 800 ppm of H_2.[46] However, there have been few reports on SnO_2-based H_2 sensors with a high sensitivity at low concentration. Accordingly, the response of 168.6 for 10 ppm of H_2 gas obtained by the present work is superior to previous ones by the SnO_2–ZnO composite materials, paving the way to the development of low-concentration gas sensors.

4. CONCLUSIONS

SnO_2–ZnO composite nanofibers were fabricated using an electrospinning technique, and their sensing capabilities for H_2 gas were investigated. XRD and TEM showed that the composite nanofibers consisted of tetragonal SnO_2 and hexagonal ZnO nanograins. The composite nanofiber sensor showed better sensing selectivity to H_2 gas than did their pure components. This paper proposed that the bifunctional sensing mechanism of the composite nanofibers is responsible for the improved sensor response to H_2, in which the reducing gas effect between the SnO_2 nanograins and the metallization effect between the ZnO and SnO_2 nanograins play an important role in enhancing the H_2-sensing behavior.

■ ASSOCIATED CONTENT

Supporting Information

Dynamic resistance curves, sensor responses, and XRD patterns of the SnO_2–ZnO composite nanofibers; schematic illustration of the fabrication of sensor device; energy band diagram of SnO_2–ZnO; and a table showing the response and recovery times of the SnO_2–ZnO composite nanofibers. Text discussing on the possible presence of solid solution. The Supporting Information is available free of charge on the ACS Publications website at DOI: 10.1021/acsami.5b01817.

■ AUTHOR INFORMATION

Corresponding Authors

*E-mail: hyounwoo@hanyang.ac.kr.
*E-mail: sangsub@inha.ac.kr.

Author Contributions

S.S.K. and H.W.K. conceived the study, designed the experiments, and prepared the manuscript. A.K., Y.J.K., and J.-H.K. performed the experiments. All authors approved the final version of the paper.

Notes

The authors declare no competing financial interest.

■ ACKNOWLEDGMENTS

This work was supported by a National Research Foundation of Korea (NRF) grant funded by the Ministry of Education, Science and Technology (MEST) of Korea (2012R1A2A2A01013899) and the International Research &

DOI: 10.1021/acsami.5b01817
ACS Appl. Mater. Interfaces 2015, 7, 11351−11358

Development Program of NRF funded by MEST (2013K1A3A1A21000149).

REFERENCES

(1) Modafferi, V.; Panzera, G.; Donato, A.; Antonucci, P. L.; Cannilla, C.; Donato, N.; Spadaro, D.; Neri, G. Highly Sensitive Ammonia Resistive Sensor Based on Electrospun V_2O_5 Fibers. *Sens. Actuators, B* **2012**, *163*, 61−68.

(2) Liu, Y.; Ding, Y.; Zhang, L.; Gao, P.-X.; Lei, Y. CeO_2 Nanofibers for In Situ O_2 and CO Sensing in Harsh Environments. *RSC Adv.* **2012**, *2*, 5193−5198.

(3) Katoch, A.; Choi, S.-W.; Kim, H. W.; Kim, S. S. Highly Sensitive and Selective H_2 Sensing by ZnO Nanofibers and the Underlying Sensing Mechanism. *J. Hazard. Mater.* **2015**, *286*, 229−235.

(4) Khan, R.; Ra, H. W.; Kim, J. T.; Jang, W. S.; Sharma, D.; Im, Y. H. Nanojunction Effects in Multiple ZnO Nanowire Gas Sensor. *Sens. Actuators, B* **2010**, *150*, 389−393.

(5) Choi, S.-W.; Zhang, J.; Akash, K.; Kim, S. S. H_2S Sensing Performance of Electrospun CuO-Loaded SnO_2 Nanofibers. *Sens. Actuators, B* **2012**, *169*, 54−60.

(6) Wang, W.; Li, Z.; Zheng, W.; Huang, H.; Wang, C.; Sun, J. Cr_2O_3-Sensitized ZnO Electrospun Nanofibers Based Ethanol Detectors. *Sens. Actuators, B* **2010**, *143*, 754−758.

(7) Song, X.; Wang, Z.; Liu, Y.; Wang, C.; Li, L. A Highly Sensitive Ethanol Sensor Based on Mesoporous ZnO-SnO_2 Nanofibers. *Nanotechnology* **2009**, *20*, 075501.

(8) Fujisawa, A.; Nishino, T.; Hamakawa, Y. Hall-Effect Measurement on Polycrystalline SnO_2 Thin Films. *Jpn. J. Appl. Phys.* **1998**, *27*, 552−555.

(9) Jimenez, V. M.; Gonzalez-Elipe, A. R.; Espinos, J. P.; Justo, A.; Fernandez, A. Synthesis of SnO and SnO_2 Nanocrystalline Powders by the Gas Phase Condensation Method. *Sens. Actuator, B* **1996**, *31*, 29−32.

(10) Shirahata, N.; Shin, W.; Murayama, N.; Hozumi, A.; Yokogawa, Y.; Kameyama, T.; Masuda, Y.; Koumoto, K. Reliable Monolayer-Template Patterning of SnO_2 Thin Films from Aqueous Solution and Their Hydrogen-Sensing Properties. *Adv. Funct. Mater.* **2004**, *14*, 580−588.

(11) Park, J.-A.; Moon, J.; Lee, S.-J.; Kim, S. H.; Chu, H. Y.; Zyung, T. SnO_2-ZnO Hybrid Nanofibers-Based Highly Sensitive Nitrogen Dioxides Sensor. *Sens. Actuators, B* **2010**, *145*, 592−595.

(12) Park, J. Y.; Kim, S. S. Growth of Nanograins in Electrospun ZnO Nanofibers. *J. Am. Ceram. Soc.* **2009**, *92*, 1691−1694.

(13) Viter, R.; Katoch, A.; Kim, S. S. Grain Size Dependent Bandgap Shift of SnO_2 Nanofibers. *Met. Mater. Int.* **2014**, *20*, 163−167.

(14) Kim, H. W.; Shim, S. H.; Lee, J. W.; Park, J. Y.; Kim, S. S. $Bi_2Sn_2O_7$ Nanoparticles Attached to SnO_2 Nanowires and Used as Catalysts. *Chem. Phys. Lett.* **2008**, *456*, 193−197.

(15) Choi, S.-W.; Katoch, A.; Zhang, J.; Kim, S. S. Electrospun Nanofibers of CuO-SnO_2 Nanocomposite as Semiconductor Gas Sensors for H_2S Detection. *Sens. Actuators, B* **2013**, *176*, 585−591.

(16) Katoch, A.; Choi, S.-W.; Sun, G.-J.; Kim, S. S. An Approach to Detecting a Reducing Gas by Radial Modulation of Electron-Depleted Shells in Core-Shell Nanofibers. *J. Mater. Chem. A* **2013**, *1*, 13588−13596.

(17) Kwon, Y. J.; Cho, H. Y.; Na, H. G.; Lee, B. C.; Kim, S. S.; Kim, H. W. Improvement of Gas Sensing Behavior in Reduced Graphene Oxides by Electron-Beam Irradiation. *Sens. Actuators, B* **2014**, *203*, 143−149.

(18) Park, J. Y.; Choi, S.-W.; Kim, S. S. A Model for the Enhancement of Gas Sensing Properties in SnO_2-ZnO Core-Shell Nanofibers. *J. Phys. D: Appl. Phys.* **2011**, *44*, 205403.

(19) Singh, N.; Ponzoni, A.; Gupta, R. K.; Lee, P. S.; Comini, E. Synthesis of In_2O_3-ZnO Core-Shell Nanowires and Their Application in Gas Sensing. *Sens. Actuators, B* **2011**, *160*, 1346−1351.

(20) Lu, G.; Xu, J.; Sun, J.; Yu, Y.; Zhang, Y.; Liu, F. UV-Enhanced Room Temperature NO_2 Sensor Using ZnO Nanorods Modified with SnO_2 Nanoparticles. *Sens. Actuators, B* **2012**, *162*, 82−88.

(21) Jinkawa, T.; Sakai, G.; Tamaki, J.; Miura, N.; Yamazoe, N. Relationship between Ethanol Gas Sensitivity and Surface Catalytic Property of Tin Oxide Sensors Modified with Acidic or Basic Oxides. *J. Mol. Catal. A: Chem.* **2000**, *155*, 193−200.

(22) Kim, K.-W.; Cho, P.-S.; Kim, S.-J.; Lee, J.-H.; Kang, C.-Y.; Kim, J.-S.; Yoon, S.-J. The Selective Detection of C_2H_5OH Using SnO_2-ZnO Thin Film Gas Sensors Prepared by Combinatorial Solution Deposition. *Sens. Actuators, B* **2007**, *123*, 318−324.

(23) Wang, Y.; Meyer, B.; Yin, X.; Kunat, M.; Langenberg, D.; Traeger, F.; Birkner, A.; Wöll, C. Hydrogen Induced Metallicity on the ZnO$(10\bar{1}0)$ Surface. *Phys. Rev. Lett.* **2005**, *95*, 266104.

(24) Wang, C.; Zhou, G.; Li, J.; Yan, B.; Duan, W. Hydrogen-Induced Metallization of Zinc Oxide $(2\bar{1}10)$ Surface and Nanowires: The Effect of Curvature. *Phys. Rev. B* **2008**, *77*, 245303.

(25) Wagner, C. D.; Riggs, W. M.; Davis, L. E.; Moulder, J. F.; Muilenberg, G. E. *Handbook of X-Ray Photoelectron Spectroscopy*; Perkin-Elmer: Eden Prairie, MN, 1979.

(26) *NIST X-ray Photoelectron Spectroscopy Database*; National Institute of Standards and Technology: Gaithersburg, MD. http://srdata.nist.gov/xps/.

(27) Moulder, J. F.; Stickle, W. F.; Sobol, P. E.; Bomben, K. D. *Handbook of X-ray Photoelectron Spectroscopy*, Chastain, J., Ed., Perkin-Elmer: New York, 1992.

(28) Slam, M. N.; Ghosh, T. B.; Chopra, K. L.; Acharya, H. N. XPS and X-ray Diffraction Studies of Aluminum-Doped Zinc Oxide Transparent Conducting Films. *Thin Solid Films* **1996**, *280*, 20−25.

(29) Pandey, S. K.; Pandey, S. K.; Deshpande, U. P.; Awasthi, V.; Kumar, A.; Gupta, M.; Mukherjee, S. Effect of Oxygen Partial Pressure on The Behavior of Dual Ion Beam Sputtered ZnO Thin Films. *Semicond. Sci. Technol.* **2013**, *28*, 085014.

(30) Bie, L.-J.; Yan, X.-N.; Yin, J.; Duan, Y.-Q.; Yuan, Z.-H. Nanopillar ZnO Gas Sensor for Hydrogen and Ethanol. *Sens. Actuators, B* **2007**, *126*, 604−608.

(31) Liangyuan, C.; Shouli, B.; Guojun, Z.; Dianqing, L.; Aifan, C.; Liu, C. C. Synthesis of ZnO-SnO_2 Nanocomposites by Microemulsion and Sensing Properties for NO_2. *Sens. Actuators, B* **2008**, *134*, 360−366.

(32) Choi, S.-W.; Park, J. Y.; Kim, S. S. Synthesis of SnO_2-ZnO Core-Shell Nanofibers via a Novel Two-Step Process and Their Gas Sensing Properties. *Nanotechnology* **2009**, *20*, 465603.

(33) Park, J.-A.; Moon, J.; Lee, S.-J.; Kim, S. H.; Chu, H. Y.; Zyung, T. SnO_2-ZnO Hybrid Nanofibers-Based Highly Sensitive Nitrogen Dioxides Sensor. *Sens. Actuators, B* **2010**, *145*, 592−595.

(34) Hwang, I.-S.; Kim, S.-J.; Choi, J.-K.; Choi, J.; Ji, H.; Kim, G.-T.; Cao, G.; Lee, J.-H. Synthesis and Gas Sensing Characteristics of Highly Crystalline ZnO-SnO_2 Core-Shell Nanowires. *Sens. Actuators, B* **2010**, *148*, 595−600.

(35) Kim, K.-W.; Cho, P.-S.; Kim, S.-J.; Lee, J.-H.; Kang, C.-Y.; Kim, J.-S.; Yoon, S.-J. The Selective Detection of C_2H_5OH Using SnO_2-ZnO Thin Film Gas Sensors Prepared by Combinational Solution Deposition. *Sens. Actuators, B* **2007**, *123*, 318−324.

(36) Song, X.; Wang, Z.; Liu, Y.; Wang, C.; Li, L. A Highly Sensitive Ethanol Sensor Based on Mesoporous ZnO-SnO_2 Nanofibers. *Nanotechnology* **2009**, *20*, 075501.

(37) Khoang, N. D.; Trung, D. D.; Duy, N. V.; Hoa, N. D.; Hieu, N. V. Design of SnO_2/ZnO Hierarchical Nanostructures for Enhanced Ethanol Gas-Sensing Performance. *Sens. Actuators, B* **2012**, *174*, 594−601.

(38) Hemmati, S.; Firooz, A. A.; Khodadadi, A. A.; Mortazavi, Y. Nanostructured SnO_2-ZnO Sensors: Highly Sensitive and Selective to Ethanol. *Sens. Actuators, B* **2011**, *160*, 1298−1303.

(39) Yu, J. H.; Choi, G. M. Electrical and CO Gas Sensing Properties of ZnO-SnO_2 Composites. *Sens. Actuators, B* **1998**, *52*, 251−256.

(40) Tang, W.; Wang, J.; Yao, P.; Li, X. Hollow Hierarchical SnO_2-ZnO Composite Nanofibers with Heterostructure Based on Electrospinning Method for Detecting Methanol. *Sens. Actuators, B* **2014**, *192*, 543−549.

DOI: 10.1021/acsami.5b01817
ACS Appl. Mater. Interfaces 2015, 7, 11351−11358

(41) Zhang, W.-H.; Zhang, W.-D. Fabrication of SnO_2-ZnO Nanocomposite Sensor for Selective Sensing of Trimethylamine and Freshness of Fishes. *Sens. Actuators, B* **2008**, *134*, 403−408.
(42) Tien, L. C.; Norton, D. P.; Gila, B. P.; Pearton, S. J.; Wang, H.-T.; Kang, B. S.; Ren, F. Detection of Hydrogen with SnO_2-Coated ZnO Nanorods. *Appl. Surf. Sci.* **2007**, *253*, 4748−4752.
(43) Huang, H.; Gong, H.; Chow, C. L.; Guo, J.; White, T. J.; Tse, M. S.; Tan, O. K. Low-Temperature Growth of SnO_2 Nanorod Arrays and Tunable n-p-n Sensing Response of a ZnO/SnO_2 Heterojunctions for Exclusive Hydrogen Sensors. *Adv. Funct. Mater.* **2011**, *21*, 2680−2686.
(44) Mondal, B.; Basumatari, B.; Das, J.; Roychaudhury, C.; Saha, H.; Mukherjee, N. ZnO-SnO_2 Based Composite Type Gas Sensor for Selective Hydrogen Sensing. *Sens. Actuators, B* **2014**, *194*, 389−396.
(45) Bie, L.-J.; Yan, X.-N.; Yin, J.; Duan, Y.-Q.; Yuan, Z.-H. Nanopillar ZnO Gas Sensor for Hydrogen and Ethanol. *Sens. Actuators, B* **2007**, *126*, 604−608.
(46) Sakai, G.; Baik, N. S.; Miura, N.; Yamazoe, N. Gas Sensing Properties of Tin Oxide Thin Films Fabricated from Hydrothermally Treated Nanoparticles Dependence of CO and H_2 Response on Film Thickness. *Sens. Actuators, B* **2001**, *77*, 116−121.

DOI: 10.1021/acsami.5b01817
ACS Appl. Mater. Interfaces 2015, 7, 11351−11358